Purdue University
Purdue e-Pubs

Open Access Theses

Theses and Dissertations

January 2015

PHOTOFLASH AND LASER IGNITION OF HIGH-NITROGEN MATERIALS

Narendra Nath De
Purdue University

Follow this and additional works at: https://docs.lib.purdue.edu/open_access_theses

PURDUE UNIVERSITY
GRADUATE SCHOOL
Thesis/Dissertation Acceptance

This is to certify that the thesis/dissertation prepared

By Narendra Nath De

Entitled
PHOTOFLASH AND LASER IGNITION OF HIGH-NITROGEN MATERIALS

For the degree of   Master of Science in Aeronautics and Astronautics

Is approved by the final examining committee:

Dr. Steven Son
Chair

Dr. Ibrahim E. Gunduz

Dr. Li Qiao

To the best of my knowledge and as understood by the student in the Thesis/Dissertation Agreement, Publication Delay, and Certification Disclaimer (Graduate School Form 32), this thesis/dissertation adheres to the provisions of Purdue University's "Policy of Integrity in Research" and the use of copyright material.

Approved by Major Professor(s): Dr. Steven Son

Approved by: Dr. Weinong Wayne Chen   11/23/2015

Head of the Departmental Graduate Program   Date

PHOTOFLASH AND LASER IGNITION OF HIGH-NITROGEN MATERIALS

A Thesis

Submitted to the Faculty

of

Purdue University

by

Narendra N. De

In Partial Fulfillment of the

Requirements for the Degree

of

Master of Science in Aeronautics and Astronautics

December 2015

Purdue University

West Lafayette, Indiana

This thesis is dedicated to my parents for all their love and support throughout my

education.

ACKNOWLEDGEMENTS

TABLE OF CONTENTS

LIST OF TABLES

LIST OF FIGURES

LIST OF SYMBOLS

I_{peak}	Peak irradiance
E''	Energy per unit flux deposited
d	Diameter
A_p	Wall area
V	Volume
δ	Flame thickness
$\dot{q}''_{cond}$	Rate of heat conduction per unit area
$\dot{q}'''_{chem}$	Rate of heat generation per unit volume
T	Temperature
$\dfrac{d\varepsilon}{dt}$	Reaction rate, ε is the reaction progress variable
k_g	Gas phase thermal conductivity
ρ	Density
α_g	Gas phase thermal diffusivity
r_b	Burning rate
r	Reflectivity
Q	Heat release per unit mass
C_p	Heat capacity
m	Mass

ABSTRACT

De, Narendra N. M.S.A.A., Purdue University, December 2015. Photoflash and Laser Ignition of Select High-Nitrogen Materials. Major Professor: Dr. Steven Son

Gas-producing energetic materials that can be readily ignited with a photoflash are typically opaque sensitive primary explosives. This study explores the photoactivity of select high-nitrogen (HiN) compounds that are much less sensitive than primary explosives. These HiN materials produce large amounts of gas upon decomposition. This makes them suitable for use in actuators, igniters, or micro-thrusters. Detailed Ignition studies were conducted using similar shaped pulses at two different wavelength ranges; specifically using a xenon photoflash and a single wavelength CO_2 laser. Several select HiN materials were tested for flash ignitability, and those that were found to be flash ignitable were further ignited with CO_2 laser heating. By comparing ignition behavior at various laser and flash intensities, some ignition mechanisms are suggested. Thermal heating, regardless of source, appears to be the dominant mechanism responsible for ignition and photochemical effects appear to be negligible in the ignition of the materials considered in this study. Higher laser and photoflash irradiance is shown to require less energy, and is therefore more efficient. The opacity of the material is an important consideration in ignitability, but not a sufficient criteria. Opaque materials that successfully propagate well in small capillary tubes are seen to be more likely to successfully flash ignite. It is suggested that this is due to the higher burning rate of these materials and also in part to the exothermic reaction occurring at or near the burning surface, rather than further from the burning surface. Both of these characteristics better allow reaction to proceed without quenching and will lead both to more successful microchannel combustion and flash/laser ignition.

CHAPTER 1. INTRODUCTION

1.1   Motivation

A gas producing secondary explosive that can be ignited using a remote, non-contact ignition mechanism will have a wide variety of possible applications. Most photoflash-ignitable gas generating energetic materials that have been considered are primary explosives, such as azides and fulminates [1]; the sensitivity of these materials limits their applications. Secondary explosives that could be photoflash ignited may find use as gas generators in igniters, micro-thrusters and micro-actuators for microscale devices, etc.

Some researchers have attempted to make gas generating secondary explosives photosensitive through the use of additives. One such attempt has been to add photosensitive carbon nanotubes into gas generating energetic materials, such as pentaerythritol tetranitrate (PETN), to create a flash ignitable mixture [2]. In part because it is a clear crystal, PETN will not flash ignite on its own. However, these flash ignitable PETN mixtures may have unacceptably high sensitivity for some non-explosive applications and the use of carbon nanotubes and other additives could introduce uncertainty from batch to batch in processing and formulation. Such additives could also make the mixture less efficient and more fuel rich, possibly increasing the likelihood of a secondary reaction with air. Since the combustion products could be inhaled in many applications, avoiding any additives such as carbon nanotubes and metals is desirable. Hence, a single compound that is flash ignitable, gas generating, and has acceptable sensitivity (not detonable) is desirable.

1.2 Remote Ignition of Energetic Materials

1.2.1 Historical Background

Non-contact ignition mechanisms can involve a wide range of electromagnetic radiation including visible light, infrared radiation (IR), microwaves, or even ionizing radiation. Research into ignition of explosives by radiation dates back to the 1950s. Eggert et al. published studies on the ignition of azides, acetylides, fulminates and perchlorates; detonations were also observed for some explosives under sufficiently high radiation intensities [3]. As far back as 1955, Nelson et al. discussed how heterogeneous flash ignitions could result in very high localized temperatures which can initiate reactions [4]. Early studies were also carried out by Bowden and Yoffee, who studied photodecomposition (direct decomposition of chemicals by absorption of light) of azides, nitrides, fulminates and perchlorates [1]. They also explored the photosensitization of silver azide by dyes and gold particles [1].

1.2.2 Recent Advances in Photoflash Ignitable Materials

More recently, research into photoflash ignition of different explosive mixtures, with a wide variety of additives, have been carried out [2]. Single-walled carbon nanotubes (SWNTs) have been extensively studied because of their high absorptivity and their unique ignition behavior when irradiated with a photoflash [5, 6, 7]. As discussed above, Maana et al. demonstrated that single wall carbon nanotubes mixed with PETN could ignite at remarkably low flash irradiance [2]. Braidy et al. experimentally showed that iron (Fe) nanoparticles embedded in SWNTs will flash ignite to produce oxides of iron [8]. Carbon nanotubes have also been added to fuel/air mixtures to allow for photoflash ignition [9]. However, metals and carbon nanotube additives may be undesirably toxic for some applications so alternatives are of interest.

High energy ball milling has also been shown to produce flash ignitable energetic materials. When micron size aluminum particles and poly-carbon monofluoride (PMF) are mechanically activated via high-energy ball milling, the resulting Al/PMF composite particles are ignitable by an optical flash [10]. This is thought to be due to the nanoscale

features produced in the milling process, similar to what is observed with nanoscale aluminum. Other additives considered to make explosives more sensitive to ignition by photoflash and lasers include gold and silver nanoparticles [11, 12].

1.2.3   Non-Thermal Mechanisms

Non-thermal ignition mechanisms for photoflash ignition have been hypothesized. Such mechanisms can involve direct photoexcitation of electrons within molecules at only certain wavelengths of light, which get preferentially absorbed [13]. This photothermal effect can directly lead to chemical breakup or the energy can degrade to heat [13]. Abboud et al. suggests that localized surface plasmon resonance enhances heating in flash irradiated aluminum nanoparticles (nAl), which in turn leads to ignition [14]. Greenfield et al. examined the photoactivity of a tetrazine derivatives of PETN known as *pentaerythritol trinitrate chlorotetrazine* (PetrinTzCl) [15]. The derivative PetrinTzCl exhibited a much higher level of photoactivity than PETN when irradiated with a 532 nm wavelength laser. It was reasoned that since tetrazine has a high heat of formation and is a good chromophore (can contribute to color, and hence absorption in the visible spectrum), tetrazine derivatives such as PetrinTzCl could possibly display direct photochemical decomposition under visible light. Other researchers reported on the photoactivity of nanoparticles of gold and other metals to UV and visible radiation due to plasmon resonance, with potential applications in engineering of metals and semiconductors [11]. Flash irradiation has also been researched as a cheap, chemical-free method for the deoxygenation reaction of graphite oxide in the bulk production of graphene based materials [16]. It is theorized that the flash creates strong photothermal and photoacoustic effects in order to start the decomposition [16].

1.3   High-Nitrogen Compounds

1.3.1   Overview

High-nitrogen (HiN) materials are a class of energetic compounds that derive most of their energy from the high positive heat of formation, released by decomposition, rather than from oxidation reactions of carbon or hydrogen, as is the case with most other energetic

materials [17]. HiN materials usually contain significant amounts of nitrogen in their molecular structure, and release large amounts of gaseous nitrogen upon decomposition, along with other gases like hydrogen [18]. With a few notable exceptions such as azides, hydrazines and tetrazines, HiN compounds are usually aromatic heterocyclic compounds with a wide variety of substituents. Research into HiN materials dates back to the late 1800s, followed by research on tetrazine and tetrazole rings by the 1950s and 1960s. Over the decades, a number of new (mostly nitrogen) derivatives based on these rings and other new structures have been synthesized and tested [19, 20, 21].

Derivatives of the tetrazine and tetrazole rings are among the most important HiN materials that have been studied. These include *6,6-bis(1H-1,2,3,4-tetrazole-5-ylamino)-s-tetrazine* (BTATz), *3,6-dihydrazino-1,2,4,5-tetrazine* (DHT) and mixed N-oxides of *3,3'-zeo-bis(6-amino-1,2,4,5-tetrazine)* [22, 18]. The tetrazole and tetrazine ring and their high nitrogen derivatives have many advantages and yield relatively clean and less toxic products [23], [24]. DAATO3.5, which is an N-oxide of *3,3'-zeo-bis(6-amino-1,2,4,5-tetrazine)* has one of the highest burning rates of organic compounds. Azides, which are molecules containing the azide R-N$_3$ functionality or salts with the (N$_3^-$) anion, are widely used HiN materials and have been used as airbag gas generators and as detonators. However, many azides are primary explosives. Another class of HiN materials consists of furazan derivatives of *3,4-diaminofurazan* (which was first synthesized in 1968). One of these derivatives includes *3,3'-diamino-4,4'-azoxyfurazan* (DAAF). Figures 1.1 and 1.2 show the molecular structure of two important HiN materials, BTATz and DAATO3.5.
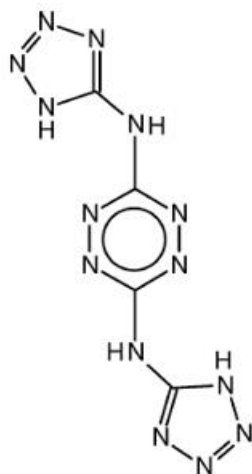
Figure 1.1 BTATz molecule [22]
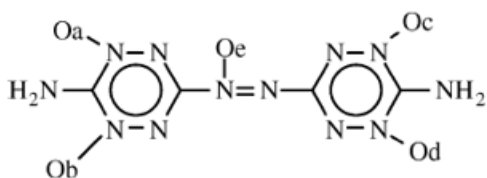
Figure 1.2 DAATO3.5 molecule [22]

A wide variety of HiN materials are synthesized by multistep routes that involve different substitute groups added to traditional aromatic rings such as the tetrazine and tetrazole ring. HiN materials such as DHT, BTATz and DAATO3.5 are all examples of such compounds. There is active research into synthesis of new HiN compounds for specific applications. Chavez et al. have studied several HiN compounds and published on the synthesis route of

nitroguanyl substitutes to the tetrazine rings [21] and of amino derivatives to the tetrazine ring [17]. International research in HiN materials include work by Sivabalan et al. who have studied the decomposition mechanisms of two gas generating HiN materials: *hydrazinium azotetrazolate* (HAZ) and *1,1′-dinitro-3,3′-azo-1,2,4-triazole* (N-DNAT) [25].

1.3.2 Properties and Potential Applications

High-nitrogen (HiN) materials have many interesting and potentially useful properties. These include reasonable insensitivity to electrostatic discharge and friction, low temperature combustion and fast burning rate in some cases [22]. In addition, most HiN materials can decompose to release a host of relatively non-toxic gaseous compounds containing nitrogen, carbon, hydrogen, and oxygen. In the case of non-azide based HiN materials, most of these gases originate from the elimination of bonds of nitrogen and the loss of other substituent groups attached to a heterocyclic base [26]. Also with the exception of azides, most HiN materials are secondary explosives or otherwise not known to detonate without strong shock initiation. BTATz and TAGzT, for example, have not been shown to be detonable. Through crystal packing, some HiN materials can also store large amounts of hydrogen. For example, *triaminoguanidinium azotetrazolate* (TAGzT) stores more hydrogen per volume than even liquid hydrogen. Decomposition pathways (different from ignition mechanisms discussed earlier) of different HiN materials can vary significantly. Bhattacharya et al. discussed how derivatives and N-oxides of the tetrazine ring have distinctly different decomposition behavior and intermediate species compared to the bare tetrazine [27]. In the decomposition of tetrazine, nitrogen (N) and hydrogen cyanide (HCN) are produced through a dissociation mechanism while the decomposition of N-oxides of the tetrazine ring, such as DAATO3.5, is different because of the different molecular structure.

Optical ignition of HiN materials could find numerous potential applications. Because of their color (opacity), many HiN materials may be more amenable to visible radiation absorption. Because of significant gas production, HiN materials could be used as low toxicity gas generators for air-bags, fire suppressants, detonators, fire extinguishers,

actuators, micro-thrusters and micro-actuators for microscale devices and as fuels in solid and reverse hybrid rocket motors [22, 18, 28].

There have also been studies in high energy nano-scale energetic materials [29], which have been seen as key to the advances in small scale application of energetics. High-nitrogen materials offer much less complexity and potentially less toxicity than metal based nano-scale energetic materials or additives. Unfortunately, studies in remote optical ignition of HiN materials are very limited.

1.3.3   Studies in Laser Ignition of High-Nitrogen Materials

Recently, a few researchers have examined the ignition of HiN materials using laser irradiation. Ali et al. [18] studied the ignition of DHT, DAAF and DAATO3.5 using a CO_2 laser. The experimental set-up included a high-speed camera and an IR detector. As expected, Ali et al. found that the differential scanning calorimetry (DSC) onset temperatures do not correspond to the laser ignition temperatures of the materials studied, but are consistent with trends. It was also shown that an exponential correlation between ignition delay and irradiance exists. No similar study of photoflash ignition of HiN materials is known to exist.

1.4   Objectives

Besides the work by Ali et al. [22, 18], very few studies have been carried out on the ignition of HiN materials by irradiation, especially in the visible spectral range. This study attempts to fill in many missing gaps in the flash ignition behavior of HiN materials.

The main objectives of this study are to:

- Determine which of the considered HiN materials are photoflash ignitable, what the ignition thresholds (lowest irradiance & energy input necessary to ignite these HiN materials) and ignition delays are.

- Determine possible ignition mechanisms by comparing ignition behavior between two different wavelengths using a photoflash and a CO_2 laser. If some HiN materials ignite while others do not, further experiments are carried out to find a cause.

CHAPTER 2.   METHODS

2.1   Photoflash Ignition Set-up and Calibration

The photoflash ignition set-up (shown in Figure 2.1) consists of a Nikon SB-24 Xenon photoflash, a sample holder, a schlieren set-up and two high speed Vision Research Phantom V7.3 Cameras, one color and one monochrome. The monochrome camera is used for schlieren imaging, while the color camera is used to record the ignition directly. The schlieren set-up consist of a diode, two mirrors and a knife edge. This set-up is consistent with what was used in previous studies [10]. The Nikon SB-24 Xenon photoflash emits a short pulse of a broadband light in the visible and near IR range [30, 31, 32]. Two layers of plastic filters, which were installed on the photoflash, were removed so that there is only one clear glass layer covering the flash.
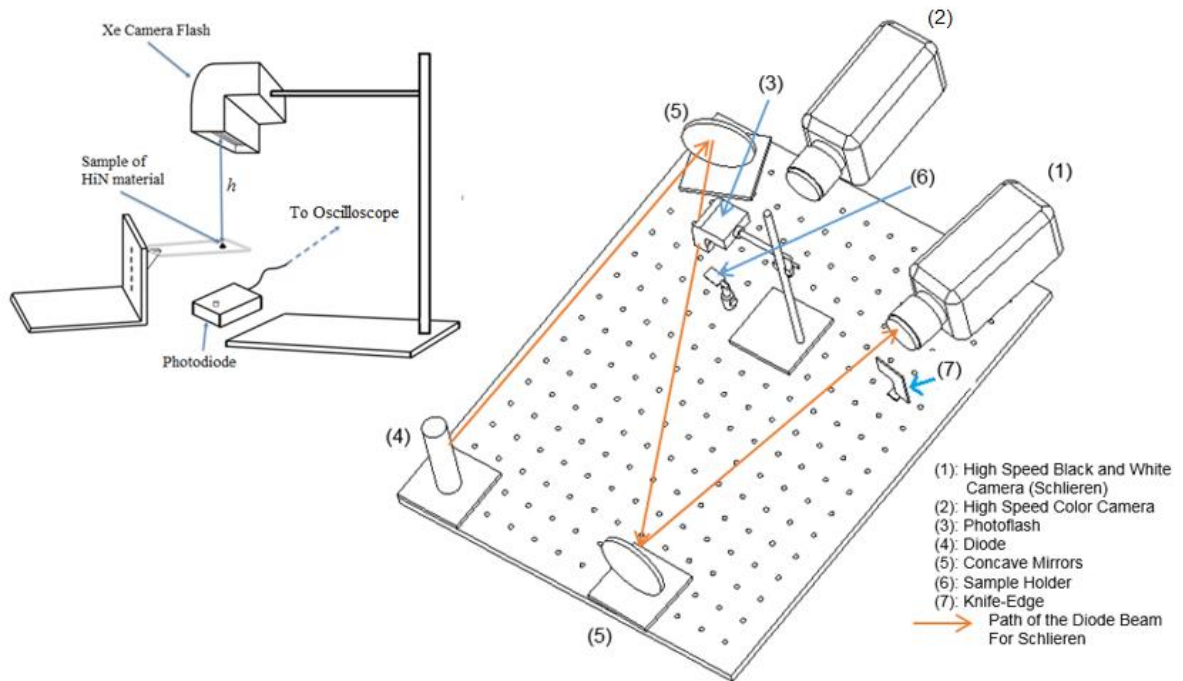
Figure 2.1 Flash calibration experimental setup

The photoflash is manually triggered and the light emitted is detected by a photodetector (ThorLabs PDA 10A). This triggers an oscilloscope, which then sends a TTL pulse to the two high speed cameras. Both cameras record at 50,000 fps.

The photoflash was calibrated using a method similar to Aslin [33]. A sample of known mass and heat capacity was flash irradiated at varying distances. The resulting temperature rise in the sample is measured using thermocouples and the heat energy irradiated by the photoflash at different heights can be determined. The thermocouples are places on the sample such that there is no direct flash irradiation to the thermocouples. A silver based thermal paste is used to ensure the thermocouples have good contact with the sample. In order to ensure the sample absorbs most of the flash irradiation, the sample is coated with soot before the experiment to maximize absorptivity. The following equation was used in order to determine the energy per unit area outputted by the photoflash,

$$E'' = \frac{C_p m \Delta T}{A(1-r)}$$
<div align="right">Eq. (1)</div>

where E'' is the energy irradiated per unit area, C_p is the heat capacity of the metallic sample, m is the mass of the sample, ΔT is the temperature rise in the sample, A is the irradiated surface area of the sample, and r is the reflectivity of the irradiated sample. In this work, r was assumed to be close to zero.

Using the lumped capacitance method described, the following plot of energy per unit area irradiated by the photoflash at different heights (h) is observed. The height (h) is the distance between the sample and the photoflash.
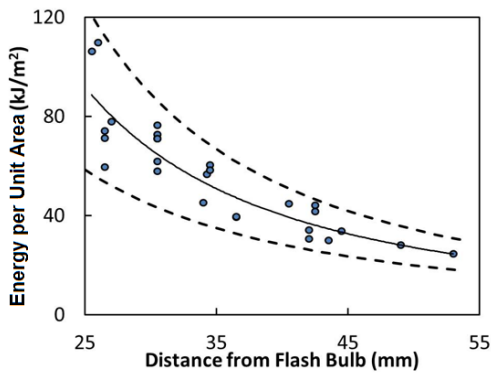
Figure 2.2 Energy per unit area irradiated by the photoflash (dashed lines are 95% confidence interval)

In order to characterize the temporal profile of the flash, a photodetector is used to obtain a plot of relative intensity with time. A neutral density filter was placed between the flash and the photodetector in order to avoid saturating the photodetector. Figure 2.3 shows the temporal profile of the photoflash.
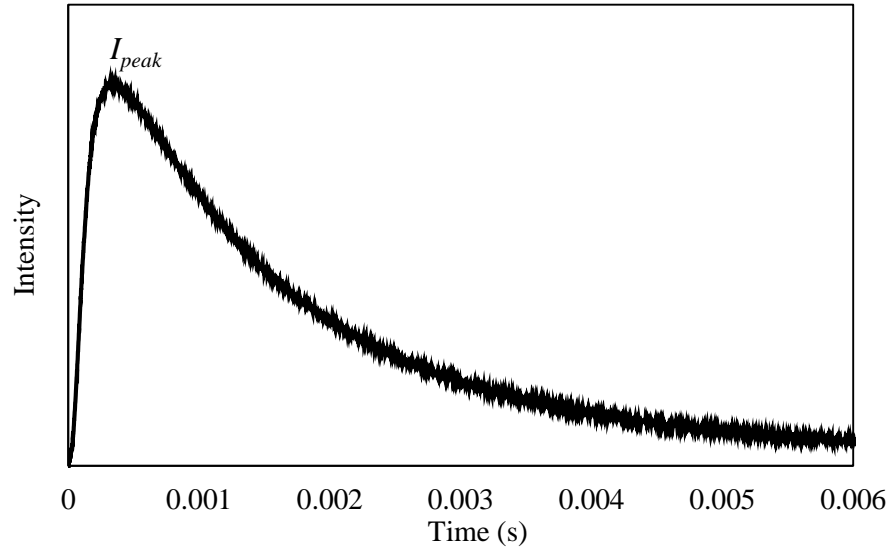
Figure 2.3 Temporal profile of photoflash

The time varying intensity profile (as shown in Figure 2.3) is directly proportional to the irradiance of the flash; therefore, the profile of the radiant intensity of the photoflash is similar to Figure 2.3. This profile could be integrated and the outcome would give the energy output of the flash,

$$E''(h) = I_{peak}(h) \times \int_0^{\sim 7ms} I(t)dt \qquad \text{Eq. (2)}$$

By normalizing this profile and integrating the flash intensity over time, a constant multiple, $\int_0^{\sim 7ms} I(t)dt$, was found which related the voltage output from the photodetector to the energy output of the flash bulb. Through this method, a peak irradiance (I_{peak}) could be determined at different stand-off distances for this flash bulb.

The HiN materials decompose and gasify with very little light emission. Hence, Ignition delays were determined using schlieren imaging. The ignition delay is the time from the trigger to the first visible onset of gasification. The ignition delay is subsequently used to determine the total energy irradiated prior to ignition, as shown in Figure 2.4. Determining the energy irradiated prior to ignition (called the ignition energy) is useful in comparing the flash and laser ignition energy thresholds.
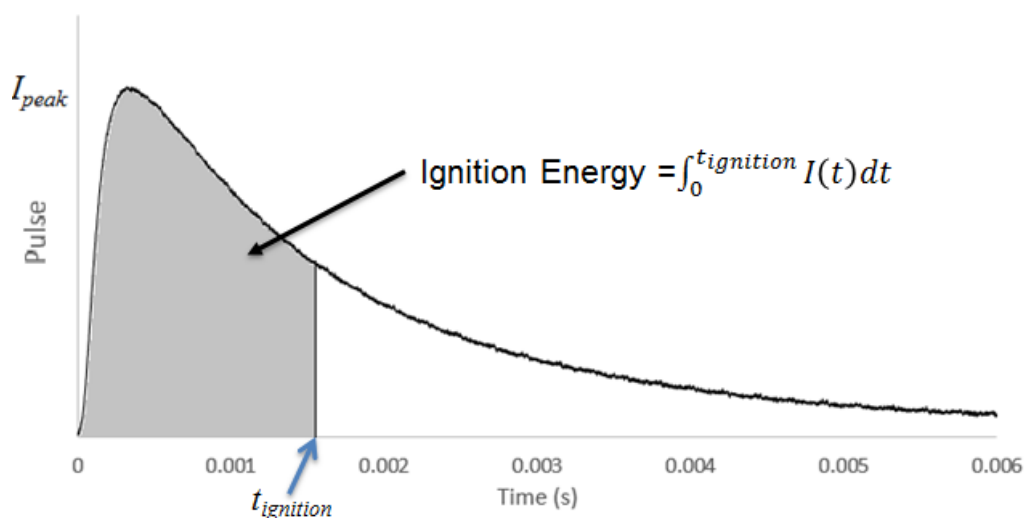
Figure 2.4 Ignition energy is the total energy irradiated prior to ignition

2.2   Laser Ignition Set-up and Calibration

The CO_2 laser (Coherent GEM 100A) setup is shown in Figure 6, The CO_2 laser wavelength is 10.6 μm. The beam is directed to the sample through a series of mirrors and is focused with a ZnSe lens with a focal length of 50 cm. A window that reflects 2% of incident laser is used to direct a small fraction of the laser energy to a beam sampler, which is used to monitor the timing of the laser pulse. The CO_2 laser is controlled by LabVIEW, and an arbitrary pulse shape and duration can be programmed. A truncated sinusoidal wave (Figure 7) with a frequency of 44.5Hz, offset by 180 degrees and with a signal duration of 6 milliseconds produces a pulse shape that was used to approximate the flash pulse profile. The total area under both the flash and the laser profiles (corresponding to the total energy per unit area) is approximately the same when the peak irradiance of each profile is equal. This is done to compare the ignition behavior of the HiN materials subjected to two similar profiles; one with a broadband photoflash and another with a laser that irradiates in far-IR spectrum.
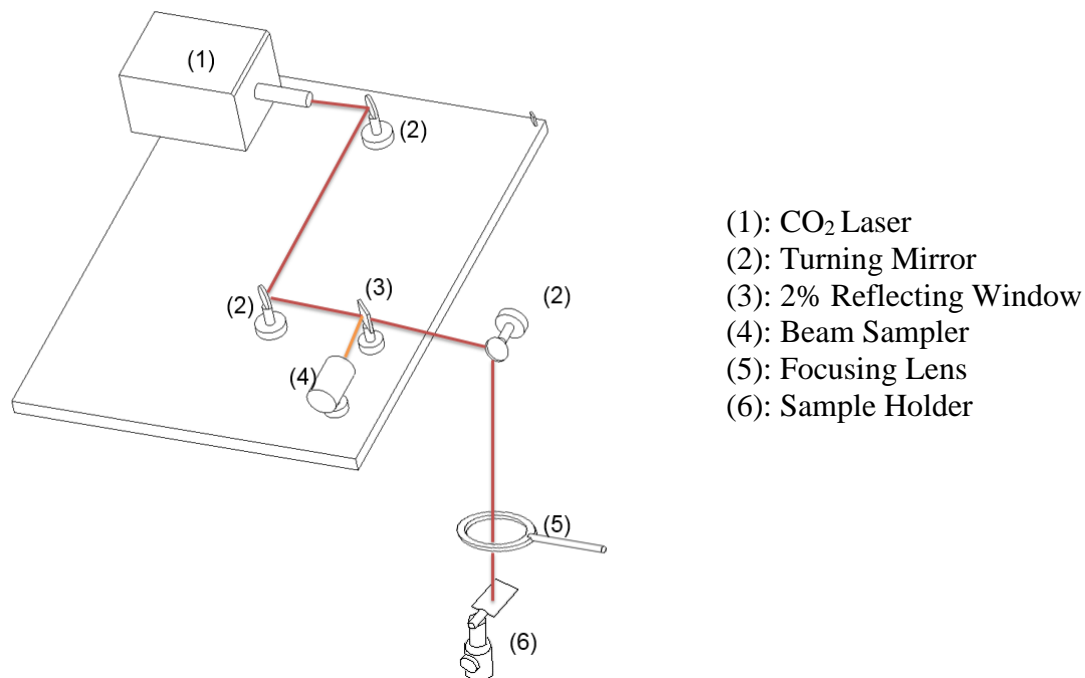
Figure 2.5 CO_2 laser profile
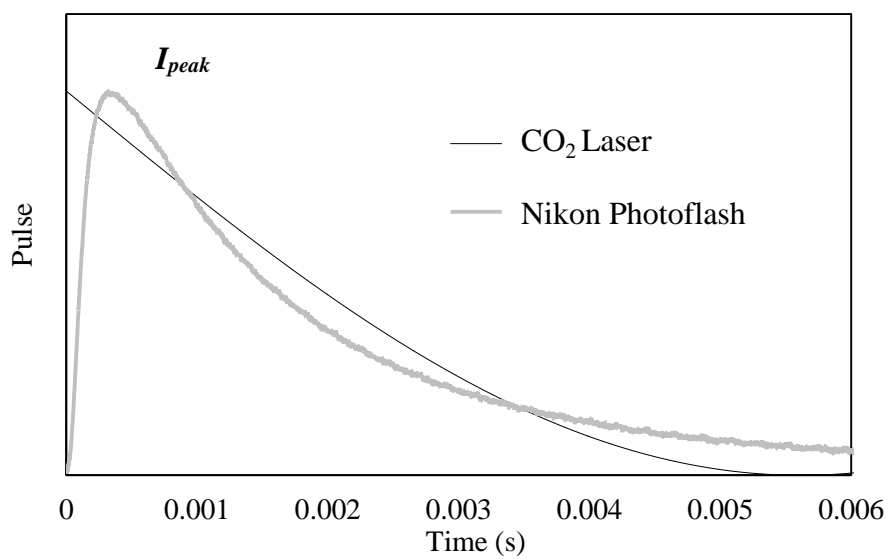
Figure 2.6 Photoflash and CO_2 laser comparison

The peak intensity is directly related to the amplitude of the pulse profile inputted in LabVIEW. A thermopile based power meter (Coherent LM-200 HTD Laser Power Detector) is used to measure the power output of the CO_2 laser. The peak irradiance can be

calculated using the measured power output and the laser spot size. The spot size was determined in previous experiments using the power meter and a knife edge. The laser outputs a Gaussian spatial profile and the edge of the spot size is defined by the radial distance from the beam center to where the irradiance drops to $1/e^2$ of the peak irradiance.

Similar to the flash setup, high-speed color video (using the color Phantom V7.3) is used for direct visual observations of the igniting particles while the monochrome Phantom is used for schlieren imaging. For the laser experiment, both cameras are triggered by a TTL signal originating from the CO_2 laser controller.

For each material, tests are selected at incremental levels which span a range of laser irradiance levels at which ignition does not occur and those that ignition occurs. Once a bound for ignition is determined, a bisection method is used to narrow down the range in which the threshold lies. This process is continued until the uncertainty in the laser power is as large as the bound between the two power settings, the average of which is the ignition threshold.

2.3   Microchannel Combustion

In order to determine how HiN materials deflagrate in small channels, samples of the HiN materials were packed in capillary tubes and ignited. This is in line with prior work [34]. Samples were loaded into capillary tubes (made from quartz glass with a 0.05 mm wall thickness) and compacted. A CO_2 laser was used to ignite the sample at the tip of the capillary tubes. Videos of the propagation and/or quenching of the flame through the capillary tube were recorded with a Phantom Miro 4 high speed camera.

CHAPTER 3. RESULTS AND DISCUSSION

3.1   Flash and Laser Ignition Results

As seen in Table 3.1, not all HiN materials flash ignited. Of the five HiN materials tested, only two, BTATz and DAATO3.5, flash ignited for the conditions considered. Reactivity is expected to play a role in successful flash ignition. Consequently, as a comparison, the DSC onset temperatures of exothermic reactions for these materials are also included in Table 3.1. Somewhat surprisingly, no correlation is apparent between DSC onset temperature and flash ignitability. Although DAATO3.5 has the lowest DSC onset temperature and BTATz has the highest, both could be flash ignited. TKX-50 is a white transparent crystal powder and scatters visible light. Consequently, it is possible that it did not flash ignite due to its low absorption at the flash wavelengths. In Table 3.2, we summarize the ignition experiments performed on those HiN that flash ignited. Videos of the laser and flash ignition can be viewed in the supplementary materials section.

Table 3.1 Flash ignitability of samples

Compound	Observed Color	DSC onset (°C)	Flash Ignitable
BTATz	Orange [35]	264	Yes
DAATO3.5	Dark Maroon [18]	177	Yes
DAAF	Orange [36]	256	No
TKX-50	White [37]	222	No
TAGzT	Yellow [35]	195	No

Table 3.2 Summary of flash experiments for BTATz and DAATO3.5

Material Tested	Flash Irradiance (I_{peak}) Range W/cm^2	Total Number of Flash Tests
BTATz	2800 – 8050	35
DAATO3.5	1500 – 6150	25

BTATz and DAATO3.5, being the only flash ignitable HiN materials, were further studied with CO_2 laser heating. Table 3.3 summarizes tests performed with the laser.

Table 3.3 Summary of laser experiments

Material Tested	Laser Irradiance (I_{peak}) Range W/cm^2	Total Number of Laser Tests
BTATz	130 – 1580	38
DAATO3.5	410 – 1610	24

Similar to the flash tests, DAATO3.5 and BTATz showed significant gasification. This made the high speed schlieren videos the best tool to observe the onset and evolution of the gasification plume. The plume development observed was similar for both the flash and the laser. Figure 3.1 and 3.2 show still images from the laser ignition while Figure 3.3 and 3.4 show still images from the flash ignition test. Scattering of unreacted particles was observed in both the laser and flash ignition (as seen in the images presented). This particle ejection is due to the rapid gasification of only a portion of the sample. The expanding gas generated causes unreacted sample to be pushed outward as some particles ignite sooner than others.

Figure 3.1 Schlieren sequence showing plume development during laser ignition of BTATz (I_{peak} = 1283.9 W/cm^2)

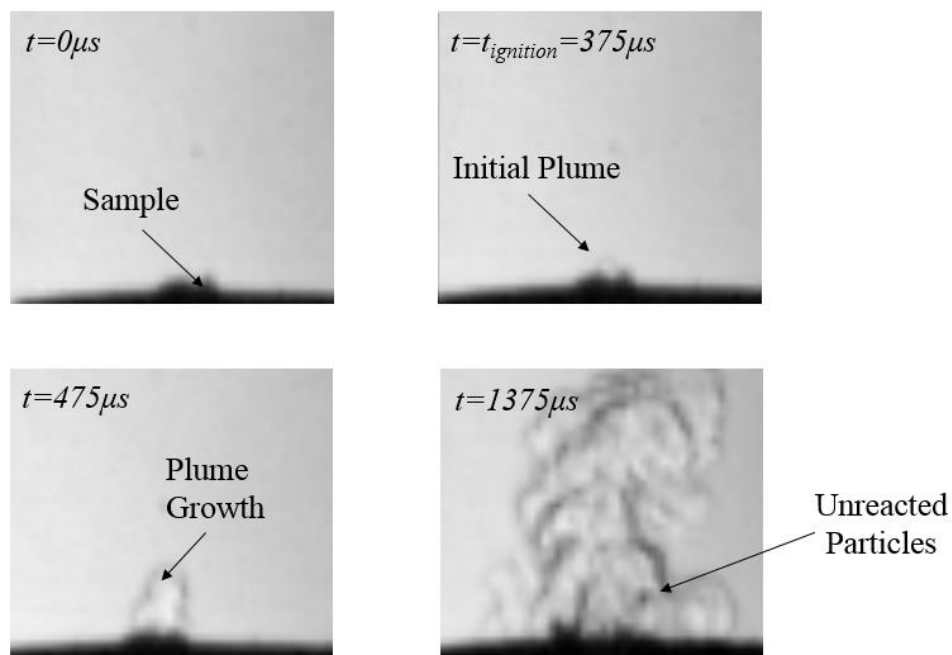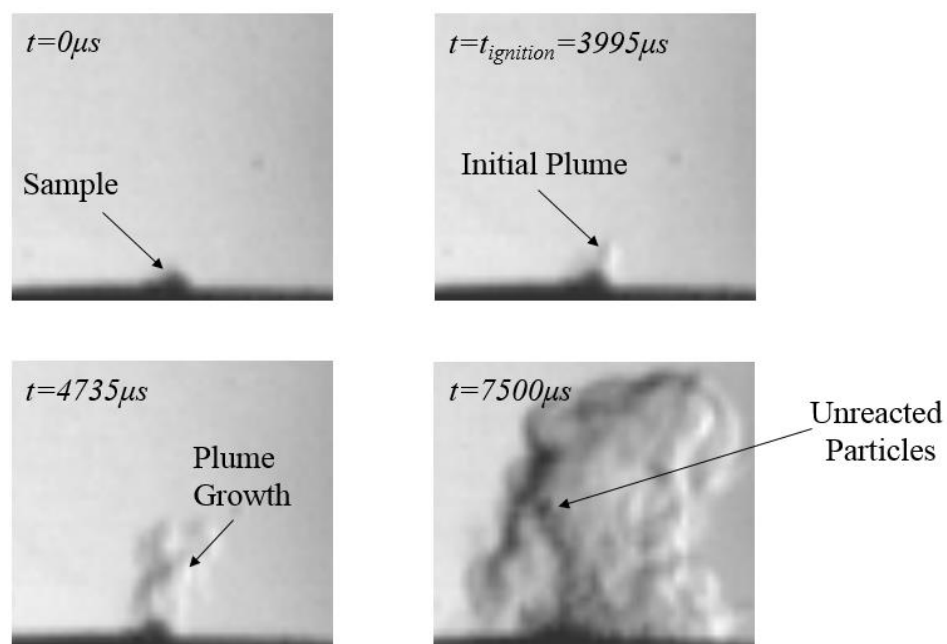Figure 3.2 Schlieren sequence showing plume development during laser ignition of DAATO3.5 (I_{peak} = 591.2 W/cm^2)
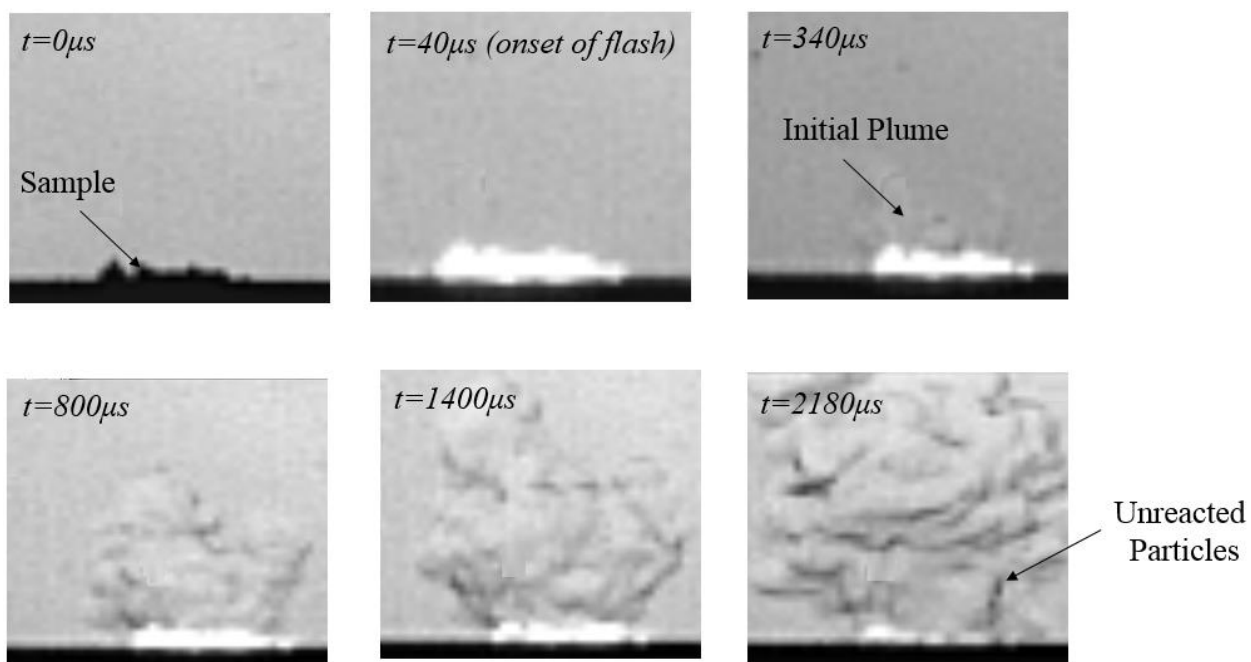
Figure 3.3 Schlieren sequence showing plume development during flash ignition of BTATz ($I_{peak} = 3730$ W/cm^2)
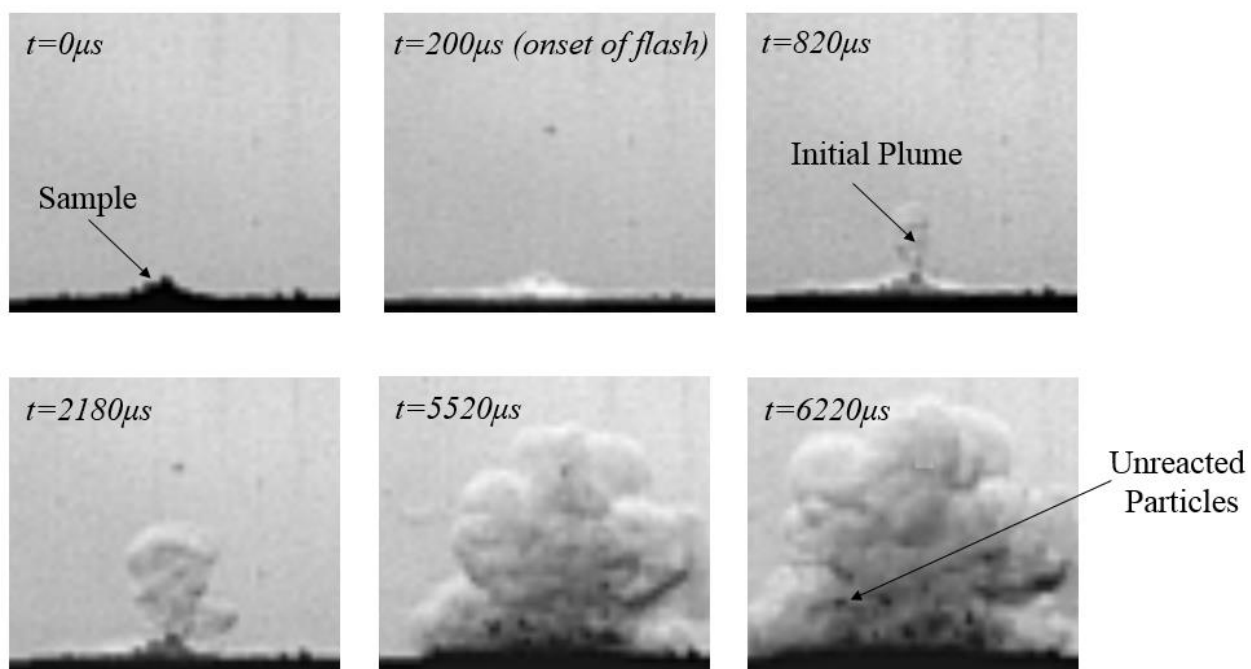
Figure 3.4 Schlieren sequence showing plume development during flash ignition of DAATO 3.5 (at $I_{peak} = 1530$ W/cm^2)

3.2   Possible Causes of Photoflash Insensitivity

Despite molecular and chemical similarities, DAATO3.5 and BTATz photoflash ignited while DAAF, TKS-50 and TAGzT did not. TKX-50 is a white transparent crystal powder and scatters incident visible light. Consequently, it is assumed that TKX-50 did not flash ignite because its absorption was low for the flash wavelengths. In previous studies with DAATO3.5 and BTATz, it was observed that these two HiN materials can successfully propagate through very small diameters [34], but other HiN materials were not reported. Therefore, BTATz, DAAF, TAGzT and DAATO3.5 were tested in the capillary tube experiment as described in the experimental set-up.

3.2.1   Microchannel Experiment

The capillary tube results (videos of which can be seen in supplementary materials) correlate with the flash ignition results in that the same two materials that successfully flash ignite can deflagrate in the capillary tubes. Only DAATO3.5 and BTATz successfully propagated in these tubes. A simple model is used to explain some of the contributing factors to quenching in small channels. Figure 3.5 shows a schematic of a flame in a small channel.
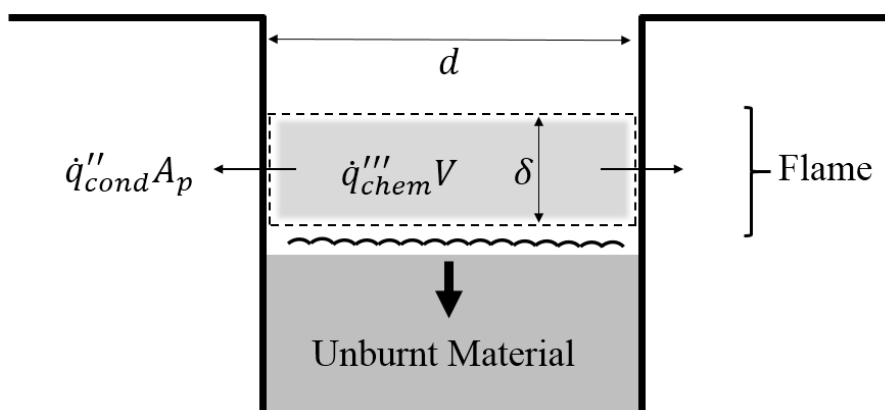
Figure 3.5 Propagation of a flame through a capillary tube

Successful propagation of a flame in a capillary tube requires the heat from the chemical reaction to overcome heat losses to the walls and ignite unburnt materials. Based on

Figure 9, a simple heat balance is derived to determine a critical diameter for combustion, d, at which the flame will quench,

$$\dot{q}'''_{chem}V = \dot{q}''_{cond}A_p \, , \qquad \text{Eq. (3)}$$

where V and A_p are the flame volume and wall area in contact with the flame, $\dot{q}'''_{chem}$ is the heat generated per unit volume and $\dot{q}''_{cond}$ is the heat conducted through the wall per unit area. Assuming Fourier conduction at the wall and a simple model for the heat release, we can write,

$$\dot{q}'''_{chem} = \frac{d\varepsilon}{dt}Q\rho \, . \qquad \text{Eq. (4)}$$

With ρ (density), Q (heat release per unit mass), ε (reaction progress variable) and k_g (gas phase thermal conductivity); substituting into Eq. (3),

$$\frac{d\varepsilon}{dt}Q\rho\frac{\pi\delta d^2}{4} = k_g\left[\frac{dT}{dx}\right]_{wall}\pi d\delta \quad \text{or} \quad \frac{1}{4}\frac{d\varepsilon}{dt}Q\rho d = k_g\left[\frac{dT}{dx}\right]_{wall}. \qquad \text{Eq. (5)}$$

The lower bound for the gradient at the wall is: $\left[\frac{dT}{dx}\right] = \frac{T_b-T_w}{d/2}$. Rearranging,

$$d = \sqrt{\frac{8k_g(T_b-T_w)}{Q\rho\frac{d\varepsilon}{dt}}} \text{ or } \propto \sqrt{\frac{1}{\frac{d\varepsilon}{dt}}} \, . \qquad \text{Eq. (6)}$$

Deflagrations have the following dependence,

$$\dot{m}'' = \rho_c r_b \propto \sqrt{\alpha_g \frac{d\varepsilon}{dt}} \, , \qquad \text{Eq. (7)}$$

where r_b is the burn rate and α_g is the gas phase thermal diffusivity. Consequently,

$$\frac{d\varepsilon}{dt} \propto r_b{}^2 \, , \qquad \text{Eq. (8)}$$

and then finally we find

$$d \propto \sqrt{\frac{1}{\frac{d\varepsilon}{dt}}} \propto \frac{1}{r_b} \, . \qquad \text{Eq. (9)}$$

Equation 9 shows that the critical diameter for combustion is inversely proportional to the burning rate. This model is consistent with the results of the capillary tube experiment and published data on the burning rates of the four HiN materials considered. Specifically, the

burning rates of BTATz and DAATO3.5 are higher than TAGzT and much higher than DAAF at 1 atm [19, 38].

3.2.2 Quenching Mechanisms

Quenching in small channels for other materials has been studied previously, where it was shown that successful propagation could also depend on where the heat is released; specifically in the gas phase or near the surface [19]. Heat release from condensed phase reactions and from reactions at or near the surface may result in less heat loss through walls. Thus, it is likely that BTATz and DAATO3.5 did not quench because of their higher burning rates and possibly due to significant near surface heat release. A similar observation has been made for nanoscale thermites in micro-channels that have significant condensed phase reactions and propagate well in microchannels [39]. When irradiated by the photoflash, it is likely that DAAF and TAGzT absorbs similar amounts of visible light compared to BTATz but do not ignite because of the failure of the initial reaction to propagate; that is, the reactions are quenched.

3.3 Comparison of Ignition Irradiance Thresholds and Ignition Energy

Figure 3.6 and 3.7 show a comparison of the irradiance at the laser and flash threshold and a comparison between ignition delay and ignition threshold. As mentioned above, the onset of ignition delay is the time between the trigger and the onset of gasification.
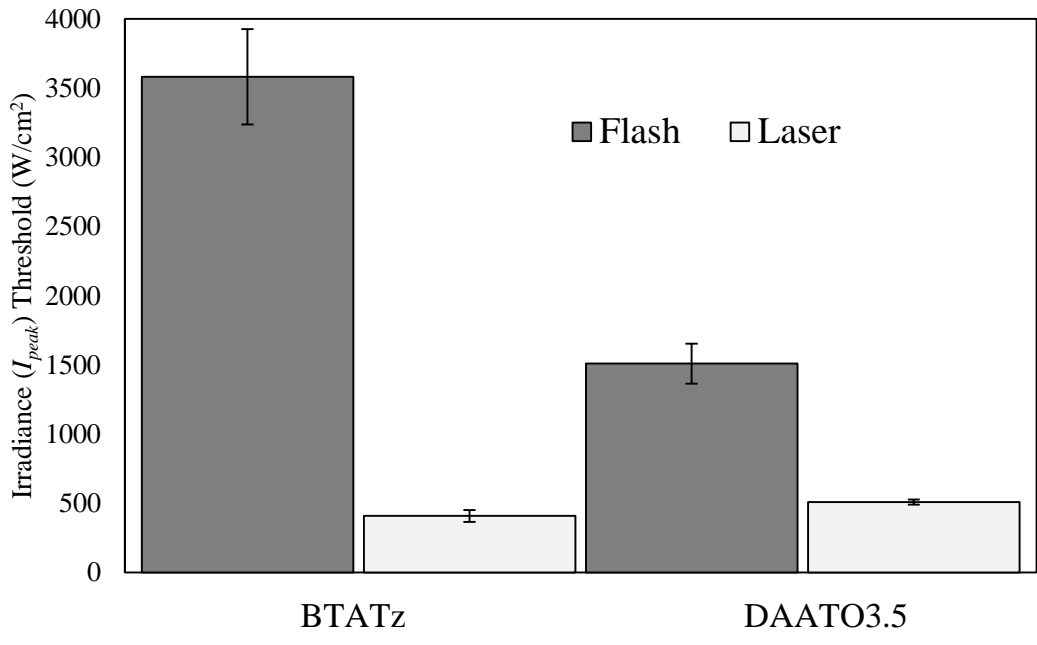
Figure 3.6 Threshold peak irradiances
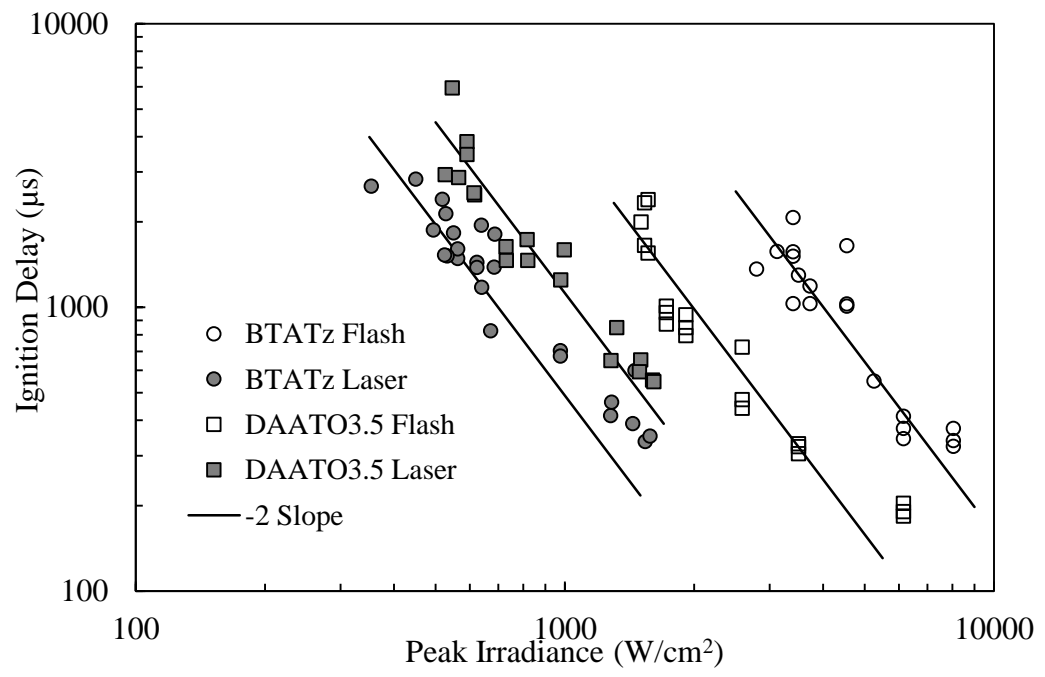
Figure 3.7 Ignition delay vs. peak irradiance for all ignition experiments

Figure 3.6 compares the threshold peak irradiances for flash versus CO_2 laser heating. The thresholds for flash ignition were significantly higher than those for the laser. This trend is also reflected in Figure 3.7, where the ignition delays are higher for the flash ignited samples at comparable peak irradiances to the laser ignited ones. Dark lines with slopes of -2 (corresponding to $t_{ignition\,delay} \propto q''^{-2}$) are imposed on the data for comparison. For every specific ignition delay, a much lower laser I_{peak} is needed to achieve ignition compared to the flash I_{peak} required for ignition. This may indicate that only a fraction of the flash energy is absorbed, compared to the laser for which absorption in the far-IR is expected to be much higher.

Both the laser and flash pulses have finite, fixed durations. However, the ignition delay of each experiment varies. Hence, comparing each experiment by the peak irradiance of the laser or flash pulse does not consider the amount of energy absorbed prior to ignition. To take this into account, the total energy per unit area irradiated prior to ignition (called the ignition energy) is calculated (using eq. 2). Figure 3.8 shows the average of the ignition energy of the experiments at the threshold while Figure 3.9 compares the ignition delay to the ignition energy for all ignition experiments.
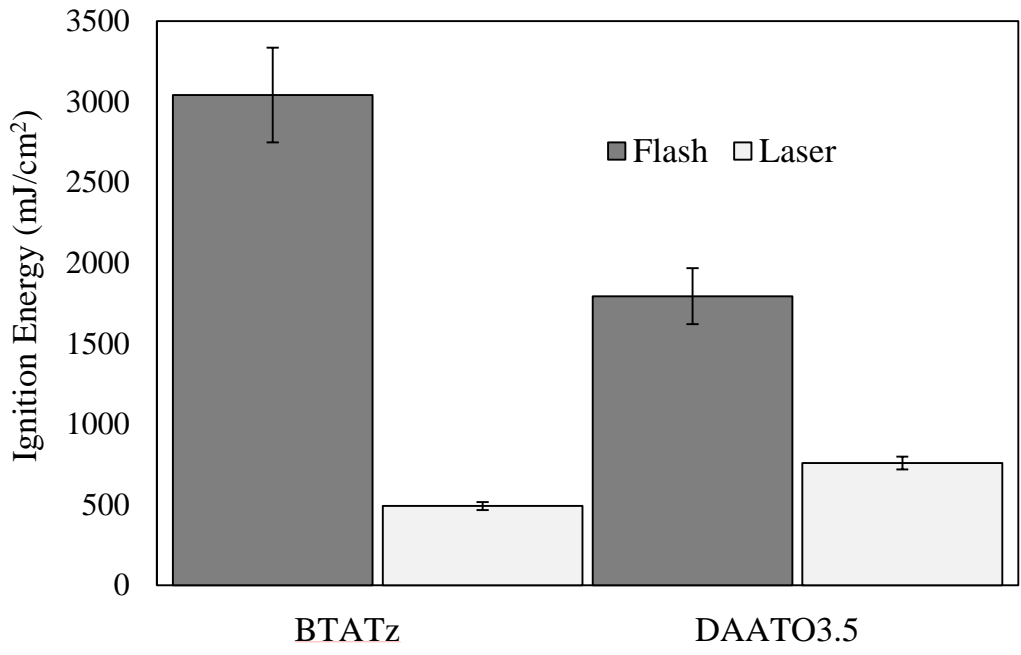
Figure 3.8 Ignition energy of pulses at threshold
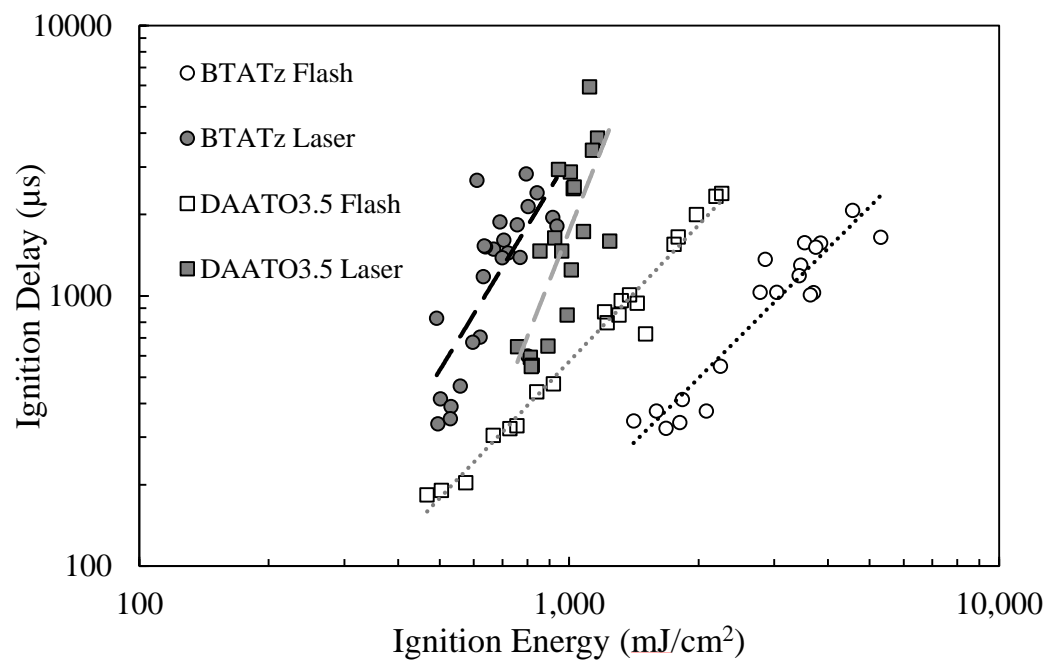
Figure 3.9 Ignition delay vs. ignition energy for all ignition experiments

3.4   Ignition Mechanisms

Both DAATO3.5 and BTATz can clearly be ignited with a lower energy and irradiance using the CO_2 laser than with the photoflash. In addition, for a given ignition delay, the peak laser irradiation and ignition energy required is a fraction of the flash ignition irradiance and ignition energy. An important and simple conclusion from these results is that the CO_2 laser is a lot more effective than the photoflash in the ignition of HiN materials. The CO_2 laser emits irradiation in the far-IR while the photoflash emits a broadband pulse that spans the visible and near IR range [30, 31, 32].

Although the power fit in the log-log plot in Figure 15 may suggest the trend could be extrapolated to higher and lower irradiances, it is very likely that this trend will break down at some point. According to Ali et al., similar tests with HMX using a CO_2 laser have shown a critical energy bottleneck such that higher irradiances will result in lower ignition delay but the ignition energy required will not drop below a critical energy level [40], and this could be explored with these materials in future work. Likewise, heat conduction and other losses will prevent ignition for low irradiances.

3.5   Absence of Photochemical Effects

Observing the differences in laser and flash ignition characteristics in Figures 3.9 and 3.10, it may be assumed that only a fraction of the photoflash energy is absorbed by the HiN materials. This is evident from the higher photoflash threshold energies compared to the laser threshold energies. These HiN materials may absorb significantly more in the IR spectrum than they do in the visible spectrum and are likely ignited by thermal heating. Photochemical effects are not anticipated at the far-IR and no indication of photochemical effects is observed for these HiN materials.

3.6   Efficiency at Higher Irradiance

It is also worth noting from Figures 3.8 and 3.10 a lower photoflash and laser energy is required to initiate ignition for those experiments at higher irradiances. For both the laser and flash ignition, the ignition energy is lower for higher irradiances, which also corresponds to short ignition delays. This could be because higher irradiances correspond

to higher rates of heating which minimize heat losses. At higher irradiances, heat conduction through the sample and into the substrate is lower. Pulses with higher irradiance are more efficient as ignition can be achieved with less energy.

CHAPTER 4. CONCLUSION AND FUTURE WORK

4.1   Conclusion

This work demonstrates, for the first time that certain, non-primary explosive, Hign-Nitrogen materials, specifically as BTATz and DAATO3.5, can be ignited using a xenon photoflash. Between these two HiN materials, DAATO3.5 is more sensitive to flash ignition than BTATz; this is likely due to its higher burning rate and its darker color, which leads to higher absorption of visible light from the photoflash.

4.1.1   Important Findings

Analysis of the flash and CO_2 laser ignition experiments show that the ignition and energy thresholds observed in laser ignitions are a fraction of that of the photoflash. Hence, it is very likely these HiN materials absorb irradiation much better in the far-IR wavelengths in contrast to the broad flash spectrum (spanning the visual and near IR). Absorption leads to thermal heating, which leads to an exothermic decomposition of the HiN material. Although photochemical effects are possible, these effects are not clearly seen in this experiment.

Additionally, ignition of BTATz and DAATO3.5 are shown to follow a trend that indicates that higher irradiances require less energy to initiate ignition. This is due to lower heat losses (less time for heat transfer) within the duration of the laser or flash pulse before ignition. This trend will likely breakdown at some point, but higher fluxes would need to be considered.

In contrast, TKX-50, DAAF and TAGzT did not flash ignite. It is assumed that TKX-50 did not flash ignite because it is a white transparent crystal powder and scatters incident visible light. Further ignition tests with the capillary tubes were carried out on BTATz, DAATO3.5, DAAF and TAGzT to compare the ability of HiN materials to propagate a reaction through a small channel. During the microchannel combustion experiment, BTATz and DAATO3.5 were observed to successfully propagate down small channels, in contrast to DAAF and TAGzT that rapidly quenched in the tube.

Upon irradiation, all of these HiN materials likely absorb similar amounts of energy, and reaction begins as microscopic hot sites. However, the observed differences are attributable to their reaction characteristics. This study did not observe a correlation to DSC exothermic onset, but did find a correlation to successful microchannel combustion. Based on the capillary tube studies, it is likely that BTATz and DAATO3.5 are sensitive to flash ignition because of their higher burning rates and because much of their chemical energy is released at the surface region during decomposition rather than in gas phase oxidation reactions. A simple analysis is used to show how the critical diameter is inversely proportional to the burning or deflagration rate. Also, because propagation in small channels depends on chemical heat release overcoming heat losses to channel walls, exothermic decomposition reactions at or near the surface as opposed to gas phase oxidation favor microchannel combustion since that would minimize the time for heat loss to the walls in the flame.

4.1.2   Possible Applications

Due to their unique photoactivity, reactivity, and acceptable sensitivity, BTATz and DAATO3.5 could be engineered for use as energetic materials in remote/non-contact ignition mechanisms. Compacts of BTATz and DAATO3.5 may be remotely ignited and a sustained combustion can occur. With additional research into implementing this technology, BTATz and DAATO3.5 have the potential to be used in gas generators, igniters, micro-thrusters and micro-actuators in micro-electro-mechanical systems (MEMS).

4.2   Future Work

One challenge in the use of aluminum micro or nano particles in energetic materials is the tendency of sub-micron and nano aluminum particles to form aggregates and clump together, thus negating all the efforts to produce the small particles. Recent development of composite mesoparticles of nAl and nitrocellulose by an electrospray process has the potential to overcome this limitation of nanoparticles. These mesoparticles consist of nanoaluminum particles within a nitrocellulose binder. This keeps the nanoaluminum particles separated and prevents formation of aggregates. Upon ignition, the nitrocellulose binder decomposes and the trapped aluminum nanoparticles ignite and are entrained in the hot, expanding gas.

Another composite energetic materials, which behaves similarly to the nAl/nitrocellulose mesoparticle, is mechanically activated aluminum and sucrose. These composite particles contains sucrose and aluminum mixed in each particle. Upon ignition, the sucrose gasifies and can ignite the aluminum particles, which get entrained in the rapidly expanding gas. This prevents any aggregate formation and allows for the dispersion of the aluminum particles. Both of these materials have the potential for use in solid propellants.

Flash and Laser ignition experiments have been shown to ignite the nAl/nitrocellulose mesoparticles and the Aluminum/sucrose composites. A flash and laser ignition study, similar to what is presented in this thesis, should be carried out on both the nAl/nitrocellulose mesoparticles and the mechanically activated Al/sucrose composite particles. This could open up the possibility of having nAl inclusions in solid propellants and the potential for flash/laser ignitable propellants.

LIST OF REFERENCES

LIST OF REFERENCES

[1] F. P. Bowden, A. D. Yoffee, Initiation and Growth of Explosions in Liquids and Solids, Cambridge University Press, U.K, 1952. 88-112

[2] M.R. Manaa, A.R. Mitchell, P.G. Garza, P.F. Pagoria, B.E. Watkins, Flash ignition and initiation of explosives-nanotubes mixture, J. Am. Chem. Soc. 127 (2005) 13786–13787. doi:10.1021/ja0547127.

[3] J. Eggert, The ignition of explosives by radiation, J. Phys. Chem. 63 (1959) 11–15.

[4] L.S. Nelson, J.L. Lundberg, Flash Initiation of Thermal Reactions, Heterog. Flash Initiat. Therm. React. 63 (1959) 433–436.

[5] X. Xiang, S. Xiang, Z. Wang, X. Wang, G. Hua, Photo-responsive behaviors and structural evolution of carbon-nanotube-supported energetic materials under a photoflash, Mater. Lett. 88 (2012) 27–29. doi:10.1016/j.matlet.2012.08.049.

[6] P.M. Ajayan, M. Terrones, A. De Guardia, V. Huc, N. Grobert, B.Q. Wei, et al., Nanotubes in a Flash — Ignition and Reconstruction, Science. 296 (2002) 705. doi:10.1126/science.296.5568.705.

[7] S.H. Tseng, N.H. Tai, W.K. Hsu, L.J. Chen, J.H. Wang, C.C. Chiu, et al., Ignition of carbon nanotubes using a photoflash, Carbon N. Y. 45 (2007) 958–964. doi:10.1016/j.carbon.2006.12.033.

[8] N. Braidy, G.A. Botton, A. Adronov, Oxidation of Fe Nanoparticles Embedded in Single-Walled Carbon Nanotubes by Exposure to a Bright Flash of White Light, Nano Lett. 2 (2002) 1277–1280. doi:10.1021/nl025718m.

[9] A.M. Berkowitz, M.A. Oehlschlaeger, The photo-induced ignition of quiescent ethylene/air mixtures containing suspended carbon nanotubes, Proc. Combust. Inst. 33 (2011) 3359–3366. doi:10.1016/j.proci.2010.07.013.

[10] T.R. Sippel, S.F. Son, L.J. Groven, Modifying Aluminum Reactivity with Poly(Carbon Monofluoride) via Mechanical Activation, Propellants, Explos. Pyrotech. 38 (2013) 321–326. doi:10.1002/prep.201200202.

[11] P. V. Kamat, Photophysical, Photochemical and Photocatalytic Aspects of Metal Nanoparticles, J. Phys. Chem. B. 106 (2002) 7729–7744. doi:10.1021/jp0209289

[12] J. M. Zucker, B. C. Tappan, D. M. Oschwald, D. N. Preston, N. J. Burnside, Characterization of Energetic Formulations Optimized for Optical Initiation Proc. 12th Int. Symp. Detonation, Coeur d'Alene, Idaho, April 11-16, (2010) 724

[13] J.S. Courtney-Pratt, G.T. Rogers, Initiation of Explosion by Light and by Flying Fragments, Nature. 175 (1955) 632–633.

[14] J.E. Abboud, X. Chong, M. Zhang, Z. Zhang, N. Jiang, S. Roy, et al., Photothermally activated motion and ignition using aluminum nanoparticles, Appl. Phys. Lett. 102 (2013) 023905. doi:10.1063/1.4776660.

[15] M.T. Greenfield, S.D. McGrane, C. a. Bolme, J. a. Bjorgaard, T.R. Nelson, S. Tretiak, et al., Photoactive High Explosives: Linear and Nonlinear Photochemistry of Petrin Tetrazine Chloride, J. Phys. Chem. A. (2015) 150507163117005. doi:10.1021/acs.jpca.5b02092.

[16] L.J. Cote, R. Cruz-Silva, J. Huang, Flash Reduction and Patterning of Graphite Oxide and its Polymer Composite, J. Am. Chem. Soc. 131 (2009) 11027–11032.

[17] D.E. Chavez, M.A. Hiskey, R.D. Gilardi, 3,3'-Azobis(6-amino-1,2,4,5-tetrazine): A Novel High-Nitrogen Energetic Material Angew. Chem., 112 (2000) 1861

[18] A.N. Ali, M.M. Sandstrom, D.M. Oschwald, K.M. Moore, S.F. Son, Laser Ignition of DAAF, DHT and DAATO3.5, Propellants, Explos. Pyrotech. 30 (2005) 351–355. doi:10.1002/prep.200500025.

[19] B.C. Tappan, A.N. Ali, S.F. Son, T.B. Brill, Decomposition and ignition of the high-nitrogen compound triaminoguanidinium azotetrazolate (TAGzT), Propellants, Explos., Pyrotech. 31 (2006) 163–168. doi:10.1002/prep.200600023.

[20] E.G. Francois, D.E. Chavez, M.M. Sandstrom, The Development of a New Synthesis Process for 3,3′-Diamino-4,4′-azoxyfurazan (DAAF), Propellants, Explos. Pyrotech. 35 (2010) 529–534. doi:10.1002/prep.200900045.

[21] D.E. Chavez, M.A. Hiskey, R.D. Gilardi, Novel High-Nitrogen Materials Based on Nitroguanyl-Substituted Tetrazines, (2004) 20–22.

[22] A. N. Ali, S.F. Son, M. a. Hiskey, D.L. Naud, Novel High Nitrogen Propellant Use in Solid Fuel Micropropulsion, J. Propuls. Power. 20 (2004) 120–126. doi:10.2514/1.9238.

[23] T.M. Klapötke, New Nitrogen-Rich High Explosives, Struct Bond (2007) 125: 85–121 doi: 10.1007/430_2007_057

[24] G. Steinhauser, T.M. Klapötke, "Green" Pyrotechnics: A Chemists' Challenge, Angew. Chemie Int. Ed. 47 (2008) 3330–3347. doi:10.1002/anie.200704510.

[25] R. Sivabalan, M. Anniyappan, S.J. Pawar, M.B. Talawar, G.M. Gore, S. Venugopalan, et al., Synthesis, characterization and thermolysis studies on triazole and tetrazole based high nitrogen content high energy materials, J. Hazard. Mater. 137 (2006) 672–680. doi:10.1016/j.jhazmat.2006.03.038.

[26] J. Oxley, Thermal decomposition of high-nitrogen energetic compounds—dihydrazido-S-tetrazine salts, Thermochim. Acta. 384 (2002) 91–99. doi:10.1016/S0040-6031(01)00780-8.

[27] A. Bhattacharya, Y.Q. Guo, E.R. Bernstein, Unimolecular decomposition of tetrazine-N-oxide based high nitrogen content energetic materials from excited electronic states., J. Chem. Phys. 131 (2009) 194304. doi:10.1063/1.3262688.

[28] J.R. Enerson, P. Richey, J.H. Lucius, Apparatus and Method for Using Tetrazine-Based Energetic Material. 20090301601. 2009.

[29] C. Rossi, K. Zhang, D. Estève, P. Alphonse, P. Tailhades, C. Vahlas, Nanoenergetic materials for MEMS: A review, J. Microelectromechanical Syst. 16 (2007) 919–931. doi:10.1109/JMEMS.2007.893519.

[30] T. Roth, J. Hohl-Ebinger, E. Schmich, W. Warta, S.W. Glunz, R.A. Sinton, Improving the accuracy of Suns-Voc measurements using spectral mismatch correction, 33rd IEEE Photovolatic Spec. Conf. (2008) 1–5. doi:10.1109/PVSC.2008.4922686.

[31] P. Rosenits, T. Roth, W. Warta, S.W. Glunz, Influence of different excitation spectra on the measured carrier lifetimes in quasi-steady-state photoconductance measurements, Sol. Energy Mater. Sol. Cells. 94 (2010) 767–773. doi:10.1016/j.solmat.2009.12.022.

[32] Y. Ohkura, P.M. Rao, X. Zheng, Flash ignition of Al nanoparticles: Mechanism and applications, Combust. Flame. 158 (2011) 2544–2548. doi:10.1016/j.combustflame.2011.05.012.

[33] H.K. Aslin, Measurement of Radiant Energy Emitted by Xenon Flashlamps, Rev. Sci. Instrum. 38 (1967) 377. doi:10.1063/1.1720709.

[34] A.S. Tappan, A.M. Renlund, G.T. Long, S.H. Kravitz, K.L. Erickson, W.M. Trott, et al., Microenergetic processing and testing to determine energetic material properties at the mesoscale, Proc. 12th Int. Symp. Detonation, San Diego, USA. (2002). http://intdetsymp.org/detsymp2002/PaperSubmit/FinalManuscript/pdf/Tappan-135.pdf.

[35] B.C. Tappan, J.M. Lloyd and V.E. Sanders, On The Shock Insensitivity of Triaminoguanidinium Azotetrazolate (TAGzT), Report No. LA-UR 09-07969, Los Alamos National Laboratories, Los Alamos, NM, USA, 2009

[36] S. Depiero, J. Koerner, J. Maienschein, R. Weese, Small-Scale Safety and Thermal Characterization of 3,3'-diamino-4,4'-azoxyfurazan (DAAF), Report No. UCRL-TR-231649, Lawrence Livermore National Laboratories, Livermore, CA, USA, 2007

[37] N. Fischer, D. Fischer, T.M. Klapötke, D.G. Piercey, J. Stierstorfer, Pushing the limits of energetic materials – the synthesis and characterization of dihydroxylammonium 5,5′-bistetrazole-1,1′-diolate, J. Mater. Chem. 22 (2012) 20418. doi:10.1039/c2jm33646d.

[38] S.F. Son, H.L. Berghout, C.A. Bolme, D.E. Chavez, D. Naud, M.A. Hiskey, Burn rate measurements of HMX, TATB, DHT, DAAF, and BTATz, Proc. Combust. Inst. 28 (2000) 919–924. doi:10.1016/S0082-0784(00)80298-2.

[39] S.F. Son, B.W. Asay, T.J. Foley, R. a. Yetter, M.H. Wu, G. a. Risha, Combustion of Nanoscale Al/MoO3 Thermite in Microchannels, J. Propuls. Power. 23 (2007) 715–721. doi:10.2514/1.26090.

[40] A.N. Ali, S.F. Son, B.W. Asay, M.E. Decroix, M.Q. Brewster, High-irradiance laser ignition of explosives, Combust. Sci. Technol. 175 (2003) 1551–1571. doi:10.1080/00102200302358.

APPENDICES

Appendix A   Calibration of the Photoflash and Laser
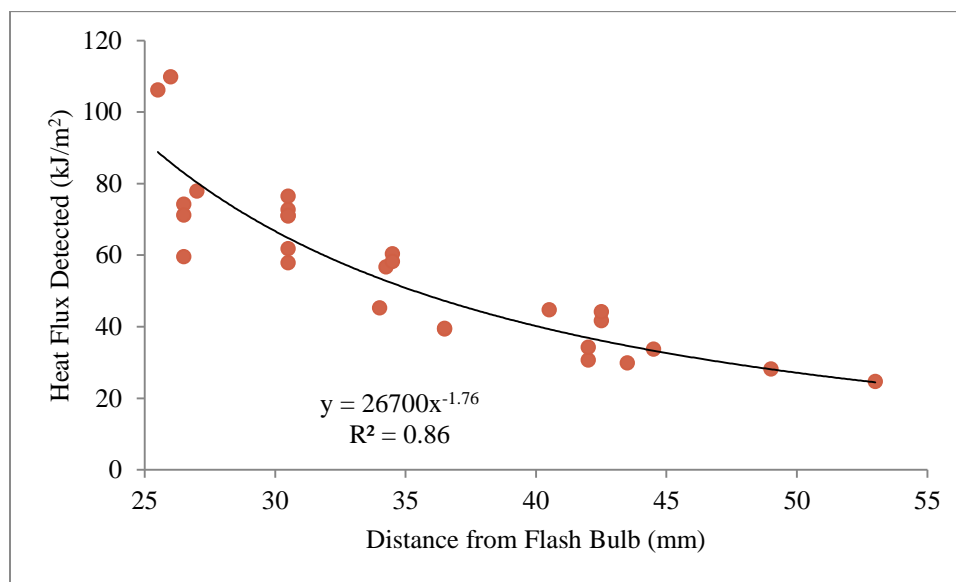
Calibration of the Photoflash

Figure A. 1 Plot of heat measured vs. distance from flash bulb for different experiments using different samples
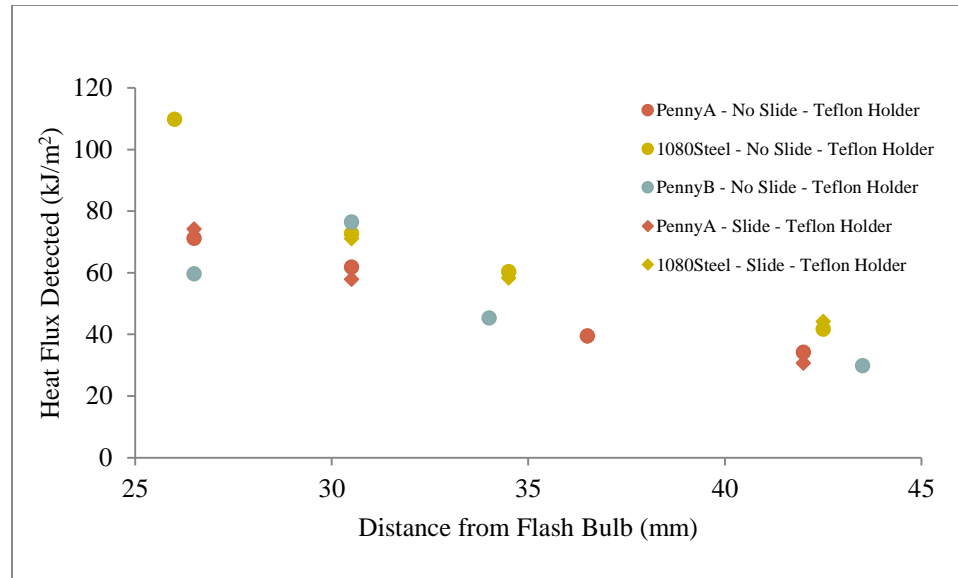
Figure A. 2 Plot of heat measured for different cases with and without a sample holder to ensure heat-loss to the sample holder is negligible

Calibration of the Laser

Table A. 1 Tabulated comparison of laser power, spot size and total irradiated energy for BTATz and DAATO3.5 laser ignition experiments

| Volt(V)	Focal Length (in)	Estimated Power (W)	Measured Laser Power (W)	Spot Size [1/e²] (mm)	Estimated Peak Irradiance (W/cm²)	Measured Peak Irradiance (W/cm²)	Total Energy Flux (J/cm^2)
5	14	57.80	32.26	1.826	1103.8	616.1	1.25
5	14	57.80	32.15	1.826	1103.8	614.0	1.24
7	14	68.32	38.25	1.826	1304.7	730.4	1.48
7	14	68.32	38.17	1.826	1304.7	728.9	1.48
9	14	73.80	42.74	1.826	1409.3	816.2	1.65
9	14	73.80	42.93	1.826	1409.3	819.8	1.66
4	16.5	50.20	26.22	1.306	1872.5	978.0	1.98
4	16.5	50.20	26.71	1.306	1872.5	996.3	2.02
6	16.5	63.78	34.35	1.306	2379.0	1281.3	2.59
6	16.5	63.78	35.4	1.306	2379.0	1320.4	2.67
8	16.5	71.60	40.27	1.306	2670.7	1502.1	3.04
8	16.5	71.60	39.99	1.306	2670.7	1491.6	3.02
10	16.5	75.10	42.92	1.306	2801.2	1600.9	3.24
10	16.5	75.10	43.23	1.306	2801.2	1612.5	3.26
2	13	29.42	15.34	2.034	452.9	236.1	0.48
3	13	40.80	22.5	2.034	628.1	346.4	0.70
5	13	57.80	31.71	2.034	889.8	488.1	0.99
7	13	68.32	36.55	2.034	1051.7	562.6	1.14
7	13	68.32	36.55	2.034	1051.7	562.6	1.14
6	13	63.78	34.29	2.034	981.8	527.9	1.07
6	13	63.78	33.63	2.034	981.8	517.7	1.05
9	13	73.80	40.51	2.034	1136.1	623.6	1.26
9	13	73.80	40.51	2.034	1136.1	623.6	1.26
10	13	75.10	43.63	2.034	1156.1	671.6	1.36
10	13	75.10	44.43	2.034	1156.1	683.9	1.38
8	13	71.60	41.54	2.034	1102.2	639.5	1.29

Appendix B   Experimental Set-up
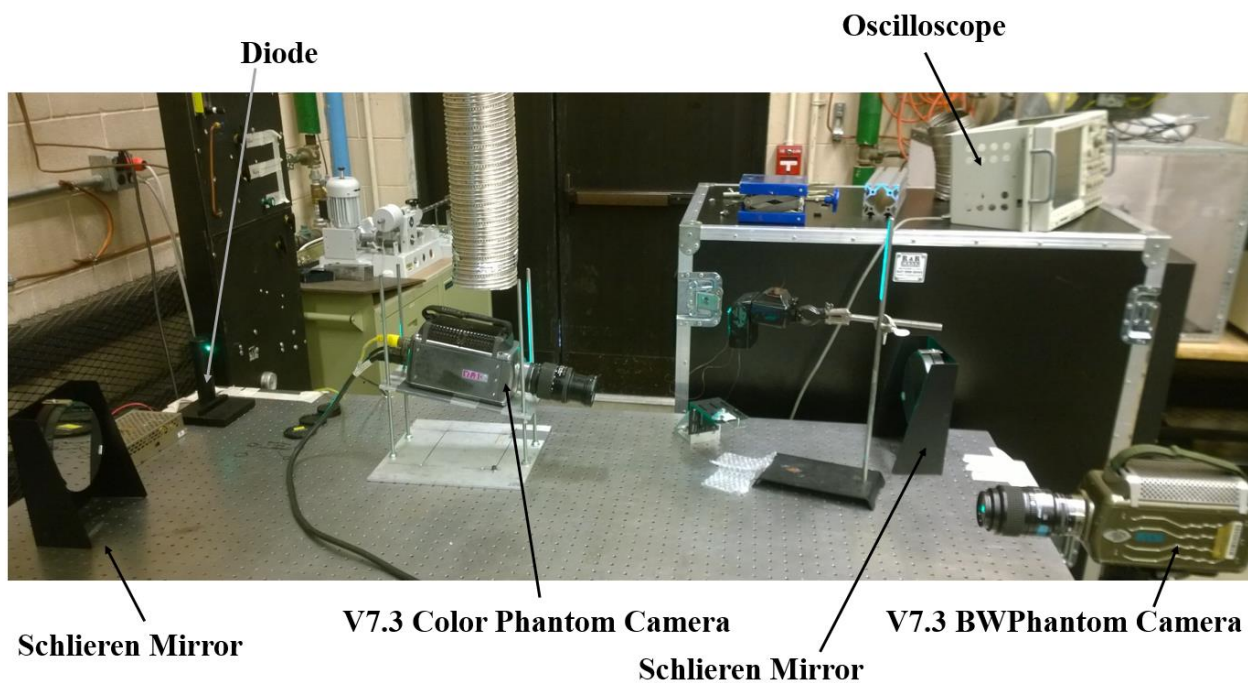
Figure B. 1 Set-up of the flash ignition experiment (lateral view)

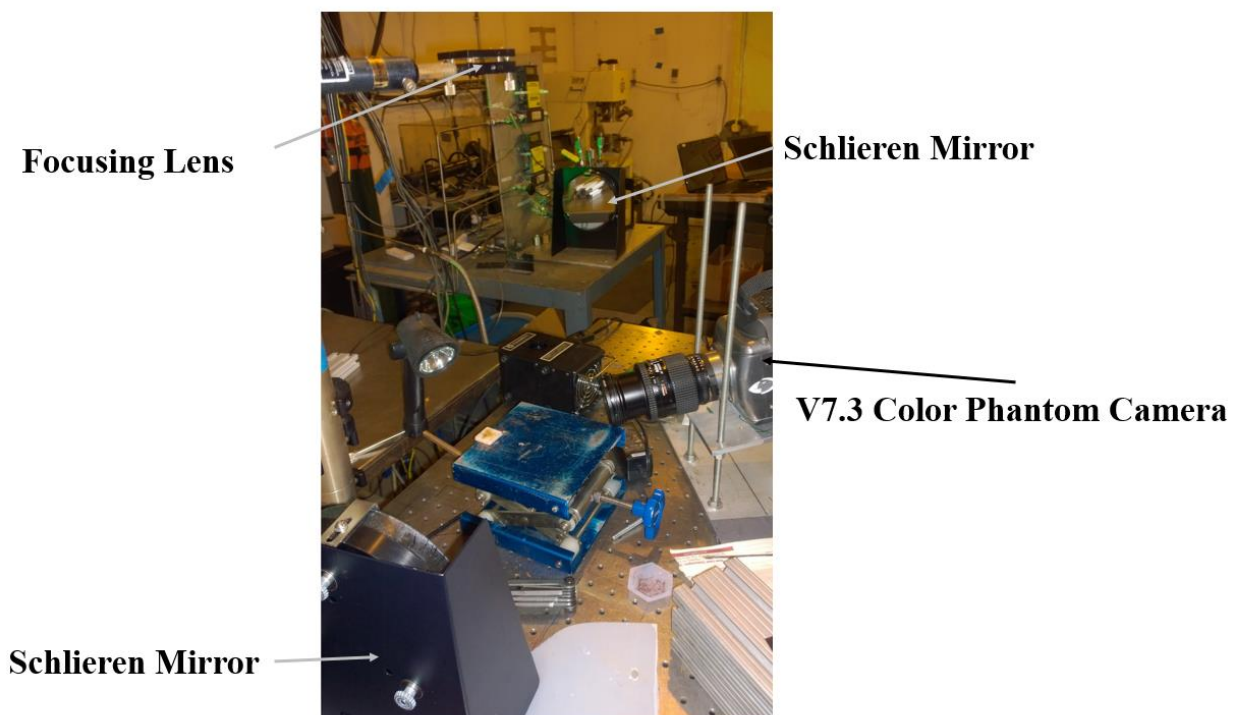Figure B. 2 Set-up of the flash ignition experiment (front view)

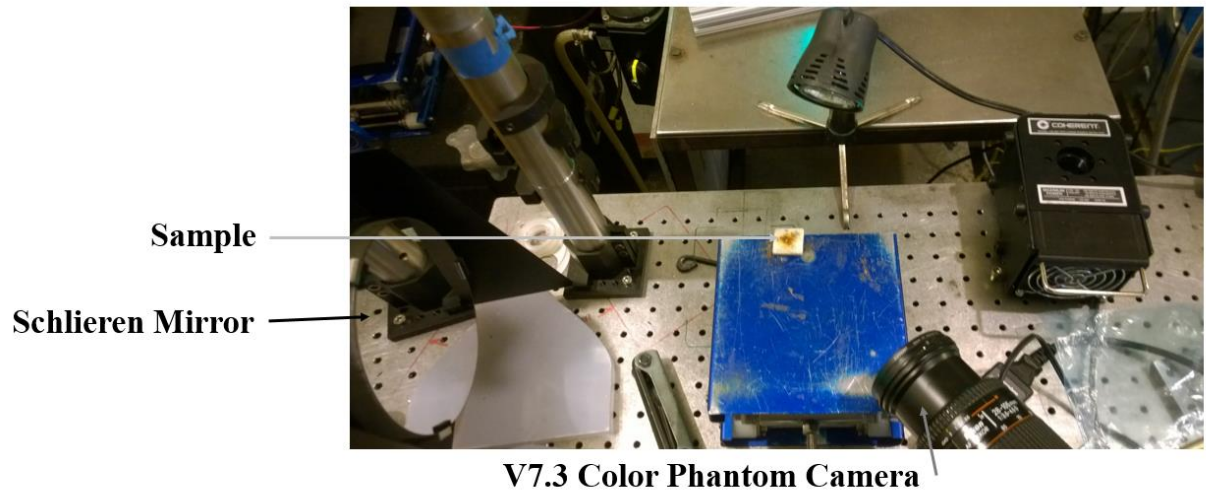Figure B. 3 Set-up of the laser ignition experiment (angled view)

Sample

Schlieren Mirror

V7.3 Color Phantom Camera

Figure B. 4 Set-up of the laser ignition experiment (top view)

Appendix C   MATLAB Scripts

Calculating energy deposited from trigger to ignition: this script calculates a constant (with units of seconds) which, when multiplied by the peak irradiance of the specific experiment, will give the energy per unit area deposited from trigger to ignition.

For the Flash Ignition Energy:

```matlab
%Profile of the Flash and Laser
A=xlsread('profile.xlsx');
Time_Laser=A(:,1);
Profile_Laser=A(:,2);

Time_Flash=A(:,4);
Profile_Flash=A(:,5);

Multiplier_Laser=0;
Multiplier_Flash=0;
%Array is the row of ignition delays inputted
for k=1:length(Array)
t_cut =Array(k)/1000000; % convert from microseconds to
seconds
time=0;
n=1;
XX=0;
YY=0;
XXX=0;
YYY=0;
%Calculate the Time from Trigger to Ignition (for the
Flash)
for n=1:size(Time_Flash)
    time=Time_Flash(n);
    XXX(:,n)=Time_Flash(n);
    YYY(:,n)=Profile_Flash(n);
if time>t_cut
    break
end
    n=n+1;
```

```matlab
end
Multiplier_Flash(k)=trapz(XXX,YYY); %Numerically Integrate
the area under the profile from Trigger to Ignition
end
```

For the Laser Ignition Energy:

```matlab
%Profile of the Flash and Laser
A=xlsread('profile.xlsx');
Time_Laser=A(:,1);
Profile_Laser=A(:,2);

Time_Flash=A(:,4);
Profile_Flash=A(:,5);

Multiplier_Laser=0;
Multiplier_Flash=0;

%Array is the row of ignition delays inputted
for k=1:length(Array)
t_cut =Array(k)/1000000; % convert from microseconds to
seconds
time=0;
n=1;
XX=0;
YY=0;
XXX=0;
YYY=0;
%Calculate the Time from Trigger to Ignition (for the
Flash)
for n=1:size(Time_Laser)
    time=Time_Laser(n);
    XXX(:,n)=Time_Laser(n);
    YYY(:,n)=Profile_Laser(n);
if time>t_cut
    break
end
    n=n+1;
end
Multiplier_Flash(k)=trapz(XXX,YYY); %Numerically Integrate
the area under the profile from Trigger to Ignition
end
```

To calculate the irradiance at ignition, the following script is used:

```matlab
A=xlsread('profile.xlsx');
Time_Laser=A(:,1);
Profile_Laser=A(:,2);

Time_Flash=A(:,4);
Profile_Flash=A(:,5);

Multiplier_Laser=0;
Multiplier_Flash=0;
%Array is the row of ignition delays inputted

for k=1:length(Array)
t_cut =Array(k)/1000000;%Converts Microseconds to Seconds
time=0;
n=1;
XX=0;
YY=0;
XXX=0;
YYY=0;

for n=1:size(Time_Flash)
    time=Time_Flash(n);
    XXX(:,n)=Time_Flash(n);
    YYY(:,n)=Profile_Flash(n);
if time>t_cut %Breaks the loop once the time is at the
ignition delay is met
    break
end
    n=n+1;
end
Multiplier_Flash(k)=YYY(n);
end
```

VITA

VITA

EDUCATION:

Purdue University, West Lafayette, IN
August 2013 to December 2015 (Expected)
Master of Science in Aeronautics and Astronautics
Major Concentration in Propulsion (Minor in Aerodynamics)
GPA: 3.9/4.0
Thesis: "*Photoflash and Laser Ignition of High-Nitrogen Materials*"

University of Texas at Arlington, Arlington, TX
August 2009 to May 2013
Bachelor of Science in Aerospace Engineering (Minor in Mechanical Engineering)

GPA: 3.72/4.0 *(Magna Cum Laude)*
Thesis: "*Innovative Structural Design of Thrust Vector Controlled Commercial Transport*"

ENGINEERING EXPERIENCE:

Los Alamos National Laboratory, Los Alamos, NM
May 2015 to August 2015
CubeSat Propulsion Development Intern

- Worked on the design, testing and data analysis of a segmented fuel/oxidizer solid propulsion system for small satellites; the system uses a high nitrogen energetic compound and ammonium perchlorate as propellants
- Helped redesign a thrust stand for the testing of a rocket motor; this included installing and calibrating a load-cell and pressure transducers
- Worked with engineers and machinist to design and construct a carbon fiber rocket motor body; this involved sizing parts, designing a pressure retaining vessel and making CAD drawings
- Analyzed test data of experiments in order to determine experimental specific impulse, thrust coefficient and mixing ratios; this data was used to model propellant burn rate characteristics
- Carried out a detailed diagnosis of possible causes for specific impulse loss
- Proposed and helped develop a flow modifier to increase fuel/oxidizer mixing
- Diagnosed non-acoustic instabilities by researching published data from small solid & hybrid motors; we fixed these instabilities by using a non-regressive graphite throat which kept the chamber pressure relatively constant

Maurice Zucrow Laboratories, West Lafayette, IN
May 2014 to Present
Graduate Research Assistant

- Studied laser and flash ignition of high-nitrogen energetic materials such as DAATO3.5, BTATz and TAGzT
- Experimentally calibrated the power output of a CO_2 laser and a Xenon photoflash
- Currently working on publishing a paper on ignition of high-nitrogen materials in the Combustion & Flame journal
- Helped other research students with a number of projects including assembling a combustion test rig, measuring solid propellant burn rate and synthesizing different energetic materials

University of Texas at Arlington, Arlington, TX
September 2010 to June 2011
Undergraduate Teaching Assistant

- Taught Pro E/CREO to a CAD laboratory class of about 30 students; this involved preparing homework and exams
  Worked extensively with Pro E/CREO in making CAD models, drawings and assemblies